

Experimental analysis of bolted, bonded, and hybrid spliced joint connections in glass fiber reinforced polymer short column

M. J. Srujan^a and Seelam Srikanth^{b*}

^aPh.D. Scholar, School of Civil Engineering, REVA University, Bangalore, India

^bAssociate Professor, School of Civil Engineering, REVA University, Bangalore, India

ARTICLE INFO

Article history:

Received 1 October 2022

Accepted 1 March 2023

Available online

1 March 2023

Keywords:

GFRP

Bonded connection

Hybrid connection Spliced

connection

Axial load

ABSTRACT

Glass Fiber Reinforced Polymer (GFRP) is a polymer composite material used in lightweight structures. This study provides insight into achieving robust GFRP H-section short-column spliced connections using bonded, bolted, and hybrid connections. The design specifications for steel splicing connections are based on BS EN 1990 and BS EN 1991 guidelines. Based on the samples subjected to axial loading, factors such as compressive strength, bonding and bearing resistance, compression behavior of the connection, and failure modes of the structure are investigated. The study includes the behavioral characteristics and results of 25 GFRP H-section Spliced connections, with each H-section measuring 152 x 72 x 6.4 mm and standing 350 mm in height. This study also examines the behavior of a composite splice joint made up of steel cover plates and steel bolts that are used to create an ideal non-bearing spliced connection. This model is used to compare to the other models to understand the behavior of spliced joints designed with GFRP cover plates. This paper holds design specifications of connections that have displayed compressive strengths of 82.35 %, 89.82 %, and 92.83 % compared to that of an un-cut GFRP H-section subjected to axial loading.

© 2023 Growing Science Ltd. All rights reserved.

1. Introduction

Fiber Reinforced Polymers (FRP) are lightweight composite materials with high strength-to-weight ratios when compared to naturally occurring metals such as steel, aluminum, copper, gold, and silver (Zhu et al., 2019; Qin et al., 2019). These FRPs are synthetically derived, and three types of FRPs are widely used in various industries: Carbon Fibre Reinforced Polymer (CFRP), Aramid Fibre Reinforced Polymer (AFRP), and Glass Fibre Reinforced Polymer (GFRP) (Zhang et al., 2016). GFRP is the most commonly used FRP in the modern construction industry due to its lower manufacturing cost compared to the other two FRPs and the material properties that GFRP exhibits when compared to traditional construction materials such as steel and iron (Figueiredo et al., 2018). GFRP is a composite material composed of high-strength glass fibers encapsulated and embedded in a thermosetting resin matrix, with fiber arrangement and orientation determined by design requirements (Quadrino et al., 2018). E-glass, C-glass, S-glass, D-glass, and L-glass are the most common glass fibers used to make GFRPs (Xu et al., 2020). E-glass GFRPs are commonly used in the construction industry for structural engineering purposes due to their high strength, availability, and low manufacturing cost when compared to other glass fibers (Gamdani et al., 2019). Because GFRPs have a high strength-to-weight ratio and are synthetic inorganic fibers, their availability and production are renewable when compared to steel or other alternative reinforcement elements used in the construction industry (Tang and Liu 2018). Because glass fibers are dense, they provide uniform load distribution and reduce micro eccentricity. The fibers also maintain dimensional stability and have a maximum elongation of 3% before failure (Santos and Campilho 2018). Pultrusion is the most cost-effective method of producing GFRP structures; with commercial pultrusion machinery, mass production of profiles similar to their steel counterparts is possible (Minghini et al., 2019). Complex GFRP

* Corresponding author. Tel.: +91 9491303992

E-mail addresses: srikanth.reddy@reva.edu.in (S. Srikanth)

ISSN 2291-8752 (Online) - ISSN 2291-8744 (Print)

© 2023 Growing Science Ltd. All rights reserved.

doi: 10.5267/j.esm.2023.3.001

shapes and designs can be assembled through the use of connection designs established through bolting, riveting, and bonding (Tsokanas et al., 2020). Composite structures are those that are made up of more than one material to function and different types of industrial composite materials have been used and developed earlier (e.g. Tao et al., 2020; Roolholamini et al., 2018; Daneshfar et al., 2017, 2023; Choupani and Torun, 2022; Hajiloo et al., 2022; Nagavally, 2017; Saeedifar and Zarouchas 2020; Karimi et al., 2023; Deng et al., 2019; Mousavi et al., 2020; Hsissou et al., 2021; Asdollah-Tabar, Gand et al., 2020; Mekonen and Bogale 2023).

The primary operational application of GFRP composites is based on their ability to exhibit high strength-to-weight ratios, weight-to-stiffness ratios, corrosion resistance, and toughness towards failure modes (Li et al., 2017). These GFRP composite design characteristics are primarily used in the aerospace, marine, petrochemical, and automobile industries to produce non-corrosive, thermal or fire-resistant, lightweight, and high-strength structures (Tao et al., 2020). Connections and joints play an important role in structural system stability, and their performance influences factors such as ductility, stiffness, and load-bearing capacity of the overall system (Ren et al., 2018). Connection problems are common when assembling a composite structure because heterogeneous connections are more difficult to work with than homogeneous connections in most cases (Tang et al., 2017). This problem can be solved by studying the connection of a specific material, applying it, and designing a composite connection (Mohan et al., 2014). When these GFRPs are combined with other building materials such as steel, iron, and concrete to create composite structures, they produce structures with a variety of advantages (Duarte et al., 2017). The main advantage of using a composite design strategy is the ability to contrast and combine different materials to create a suitable connection (Kreling et al., 2013, Fischer et al., 2013). RCC is a popular composite structural design combination in which concrete has high compressive strength and steel has a good tensile strength (Iqbal et al., 2017). Steel and GFRP can also be used for composite connection design, with steel providing the required elongation ability, tensile strength, malleability, and so on, and GFRP providing electrical resistance, thermal non-conductivity, fire resistance, good strength-weight ratio, and so on (Golewski and Sadowski 2017; Paroissien et al., 2017). Furthermore, because GFRP profiles have a low young's modulus of about 30 GPa (depending on the type of GFRP used), it is advantageous to use semi-rigid connections established using steel in the connection design to improve overall structural and joint stiffness (Chandregowda and Reddy 2018).

When designing composite connections, it is critical to examine the standard connections of the materials in their homogeneous state (Zhang et al., 2019; Xu et al., 2019). Steel, in other words, can be bolted, riveted, and welded (Ezzine et al., 2018). GFRP, on the other hand, can be bonded, bolted, and riveted (Ascione et al., 2017). The common factor between the two materials is their ability to be connected using bolts and rivets. There is also a design possibility of establishing a Hybrid connection, in which a bonded and bolted connection can be used concurrently to increase joint strength and produce more plastic hinges (Sadowski et al., 2018; Chowdhury et al., 2016). Because of its unusual nature, a hybrid connection has several advantages over a homogenous connection (Armentani et al., 2018; Marannano and Zuccarello 2015). A bonded connection, for example, has a larger surface area for load distribution than a bolted or riveted connection, which distributes the load through the bolts or rivets used in the connection (Li et al., 2020). Bonded joints are also more resistant to compression and shear, with less tolerance for tension, cleavage, and peeling or ripping-off forces (Sadowski et al., 2015; Jia et al., 2016; Galvez et al., 2019). Similarly, bolted connections are more resistant to buckling or multi-axial loading than bonded connections (da Silva et al., 2017). As a result, establishing a hybrid connection using a combination of bonded and bolted connections will provide superior connection designs when compared to homogenous connections (Lopez-Cruz et al., 2017).

Various studies on the behavior and performance of GFRP column-column connection joints have indicated that there is only a limited improvement in the mechanical properties of joints created using connectors such as cover plates with bolted connections, bonded connections, and hybrid connections (Omar et al., 2018; de Sousa Marques et al., 2019). Because of their characteristic of failing abruptly at maximum loading, the concept of robustness is critical in establishing GFRPs as a construction material. GFRPs have a 3% elongation before failure, compared to steel, which has a variety of stress-strain behaviors such as elastic behavior, elasto-plastic behavior, and plastic behavior (Ribeiro et al., 2016). To improve the joint capacity of the connection and to keep the concept of robustness in mind, non-bearing spliced joint connections are established by connecting two 350mm height GFRP H-section short columns in this research paper. Axial loading is used to investigate behaviors such as load-bearing capacity, maximum joint displacement at failure, compressive strength, stiffness, and failure modes. The efficiency of each connection was calculated by comparing the ultimate load-bearing capacity of each connection with the ultimate load-bearing capacity of an uncut GFRP structure.

2. Experimental program

The non-bearing spliced connections are designed and modeled, and the short columns assembly is made up of two GFRP H-sections with dimensions of $152 \times 76 \times 6.4$ mm and a height of 350 mm. Each specimen is designed based on the presence of a set of web cover plates, outer-flange cover plates, and inner-flange cover plates, as well as 16 M8 8.8-grade steel bolts. Each model's design is derived from a non-bearing spliced connection design following the steel standards for connection design from BS EN 1990 and BS EN 1991. To satisfy the concept of robustness, a 25 mm splicing cap is provided between the H-sections to prevent the joint from failing abruptly. This study established three types of connections: bolted, bonded,

and hybrid connections as shown in Fig. 1. Furthermore, various aspects of the connections are established based on these three connections to design and obtain 5 models, and 5 samples for each model are constructed and tested to better understand the joint behavior of each connection. Model-1 (M1) steel cover plates are held in the web, inner- and outer-flange regions and the connection is made with 20 M8 8.8 grade steel bolts. To understand the impact of cover plate material on the spliced joint, Model-2 (M2) is created by replacing the steel cover plates from model-1 with GFRP cover plates. Because the young's modulus of GFRP is lower than that of steel, bearing values will have a significant impact as a failure mode, which can be understood by testing model-2 samples. According to the BS EN 15048 standards for M8 8.8 grade steel bolts, both model-1 and model-2 bolts are tightened to a torque value of 28.4 Nm (Sadowski & Golewski 2014).

Model-3 (M3) and Model-4 (M4) are bonded connections, with GFRP cover plates used for assembly. Model 3 has a 2 mm thick bond between the cover plates and the H-section, which is considered the supplier's minimum industrial standard. Model-4 has a 5mm thick bond connecting the cover plate and the GFRP H-section; the thickness of the cover plate is 5mm, and having a bond thickness of 5mm is similar to having thicker cover plates; it also promoted the homogeneous behavior of both the cover plate and the H-section because they are made of the same material. The loading conditions, bond thickness, and bond curing environment all have a significant impact on bond strength (Ma et al., 2018; Benedetti et al., 2016). By increasing the bond thickness, strain and load are spread out over a larger surface area, resulting in lower strain concentration at the expense of increased overall joint stiffness. Model-5 (M5) is a Hybrid connection that combines bonded and bolted components. Model-5 samples are designed after testing model-2, model-3, and model-4 samples, and specifications for model-5 are generated using the data from these models' behavioral characteristics. When compared to the 2 mm bond, the 5 mm bond connection showed excellent load-bearing capacity and overall joint behavior. As a result, a 5 mm bond is being considered for the Hybrid connection. Twenty M8 8.8 grade steel bolts, similar to those used in model-2, are used to establish the bolted connection aspect of the hybrid connection. After the 5 mm thick bond is established, holes are drilled in the cover plates and the GFRP H-section to accommodate the bolted connection smoothly. According to the BS EN 15048 standards for M8 8.8 grade steel bolts, all bolts are tightened to a torque value of 28.4 Nm.

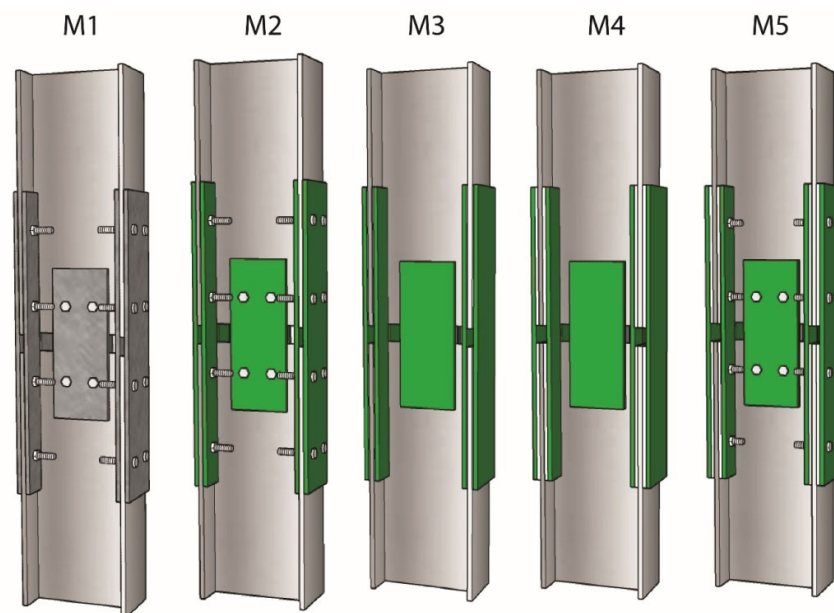


Fig. 1. Designs for model specimens

According to BS EN 1993-1-9, the thickness of the bolts used for connection should be greater than 75% of the combined thickness of the flange and flange cover plates for steel splicing connections. As a result, M8 bolts are used to create both bolted and hybrid connections. Similarly, the pitch and edge distance are calculated using the cover plate dimensions. The web plate measures 205x80 mm, while the inner and outer flange plates measure 410x150 mm and 410x76 mm, respectively. According to BS EN 1993, the pitch value for splicing connections should be greater than twice that of the edge value ($\text{pitch} > 2 \times \text{edge}$). If this criterion is not met, the thickness of the cover plates should be increased, and the bolt dimension should be adjusted accordingly. The edge value of the inner flange cover plate is 51.25 mm, and the pitch value is 102.50 mm. The edge-1 value of the outer flange cover plate is 15 mm, the pitch-1 value is 45 mm, the edge-2 value is 51.25 mm, and the pitch-2 value is 102.50 mm. Edge-1 is 20 mm, Pitch-1 is 40 mm, Edge-2 is 51.25 mm, and Pitch-2 is 102.50 mm for the web cover plate. The GFRP H-sections purchased were 1200 mm long and were all cut down to 350 mm using an industrial saw to achieve a smooth cut surface and avoid any eccentric loading during testing. Five 350 mm long un-cut short columns were crushed using axial loading to determine the load-bearing capacity of GFRP short columns and to compare the strength of an un-cut structure to the connections established in this study.

3. Test Program

The holes are drilled in the cover plates and the H-section using a stencil created based on the pitch and edge values specified in BS EN 1993-1-9 design standards for steel splicing connections. For each sample created in this study, holes are drilled with a mechanical drill while clamping the cover plates and H-sections to a working table to maintain accuracy in bolting locations. Bolt holes of 8.5mm in diameter are drilled to accommodate M8 8.8 grade bolts smoothly, resulting in a 0.5mm clearance. The minimum bolt-hole clearance recommended as an industry standard is $1.012d$ for bolted connections (Liu et al., 2018), but in the case of this study, the drill bit with that specific hole dimension was not available. As a result, based on the availability of the drill bit, the other best alternative is considered, and 8.5mm bolt holes are drilled in each of the bolted connections, and the bolts are accommodated in the bolt holes using washers to achieve the perfect bolted connection. Surface preparation is carried out to establish the bonded connections by roughening the surfaces of the GFRP H-section and the cover plate with sandpaper (Palmieri et al., 2016). The adhesive used is epoxy with a compressive strength greater than 60 N/mm^2 , tensile strength greater than 2 GPa, bond strength 6-10 N/mm^2 , and flex strength greater than 70 N/mm^2 for a 2 mm thick bond. The thickness of the bond is maintained by casting the H-section with the cover plates on top and using clamps to restrict any movement of the model that could result in an uneven bond thickness. To avoid adhesive leakage due to gravity, each surface is allowed to cure for a minimum of 48 hours before preparing the next surface. For 5mm thick bonds, the casing is marked, and air drying is performed after pouring the adhesive on each surface of the GFRP material before joining the surfaces. Because 5 mm thickness is significantly large and difficult to obtain due to the lack of complex molds or retainers, air drying is regarded as the next best alternative for curing or drying out the adhesive to establish a bond or, in other words, a homogeneous layer of connection between the two surfaces.

After testing all of the connections mentioned above, hybrid connections are created, and a 5 mm thick bonded connection is used to create the hybrid model. After the 5 mm, thick bonded connections have been established, holes are drilled through the cover plates and the H-section to accommodate the bolted connection. To avoid peeling off, delamination, or distortion in the bond connection, high-speed drills with sharp drill bits are used to reduce vibration in the connection (Wang & Melly 2018; Phadnis et al., 2013). Tightening the bolts to a torque value of 28.4 Nm compressed the bond and reduced the bond thickness near the bolt locations compared to the ledge region of the section, but the undulation is less than 1 mm as measured with a screw gauge.



Fig. 2 Test arrangement using Avery 5000

The fully assembled models are loaded into an AMSLER compressing machine as shown in Fig. 2 that is linked to an Avery 5000 kN load cell. The load is applied hydraulically, with the load cell linked to a computer to record and maintain a

consistent loading rate of 0.2 kN/s. Before applying the load, a pair of Linear Variable Differential Transformers (LVDT) with maximum displacement readings of 25 mm are installed on opposite sides of the H-section and calibrated to zero displacements. Both LVDTs are linked to a computer, which records displacement readings every second, providing an accuracy of noting down the loading and displacement simultaneously every second until the maximum load-bearing capacity or point of failure is reached.

4. Results and Discussion

To understand the compressive strength and load-bearing capacity of GFRP H-section short columns, uncut GFRP H-sections of height 350 mm are crushed under axial compression loading. The un-cut GFRP short columns failed solely due to crushing, as shown in Fig. 3, and all of the samples had large cracks, primarily at the web and flange junction. The average compressive strength is calculated to be 122.18 N/mm² with a maximum load-bearing capacity of 227.74 kN.



Fig. 3 Failure observed in the control sample

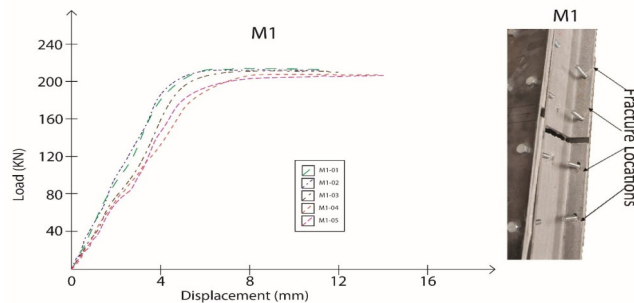


Fig. 4. Load versus displacement graph and failure modes observed in the model-1

As previously stated, model-1 is based on the strongest splicing connection conducted based on cover plate positioning. The maximum average load bearing capacity is calculated to be 211.4 kN, with a maximum displacement of 12.33 mm. The specimens from this model have an average compressive strength of 113.43 N/mm² with average bearing stress of 412.52 N/mm² per bolt hole at failure load. The stiffness is calculated by taking the slope values from the load versus displacement graph at 30% and 50% of the maximum load, as shown in Fig. 4. The average stiffness is calculated to be 24.76 kN/mm, with a force of 21 kN per bolt. The failure was caused primarily by cleavage cracks in the lower flange region, and the bolt bearing length varied between 2 mm and 8 mm.

Table 1. Specimen's characteristic properties of model 2

Sample ID	Ultimate load (kN)	Displacement at failure (mm)	Stiffness (kN/mm)	Force per bolt (kN)	Compressive strength (N/mm ²)	Bearing stress (N/mm ²)	Modes of failure
M2-01	189.3	15.8	21.2	18.93	101.50	368.25	Bearing and Net Tension
M2-02	188.4	16.1	20.9	18.84	101.02	366.50	Bearing and Net Tension
M2-03	187.9	16.8	20.1	18.79	100.75	365.52	Bearing and Net Tension
M2-04	187.1	17.1	19.6	18.71	100.32	363.97	Bearing and Net Tension
M2-05	185.6	17.2	19.0	18.56	99.52	361.05	Bearing and Net Tension
Average	187.7	16.6	20.2	18.77	100.62	365.06	

Load transfer occurs in the web and flange region in model-2 samples, with 20 bolts transmitting load from the top section of the joint to the bottom section and cover plates providing bearing resistance. The experimental results and load versus displacement graph of the model-2 samples were given in table 1 and Fig. 5 respectively. The average maximum load at failure is calculated to be 187.7 kN, resulting in a failure displacement of 16.6 mm. The average stiffness is calculated to be 20.2 kN/mm, with a compressive strength of 100.62 N/mm² on average. The failure of the connection in these samples is primarily caused by bearing and net tension in the joint as shown in Fig. 6, with bearing lengths ranging from 5 mm to 15 mm.

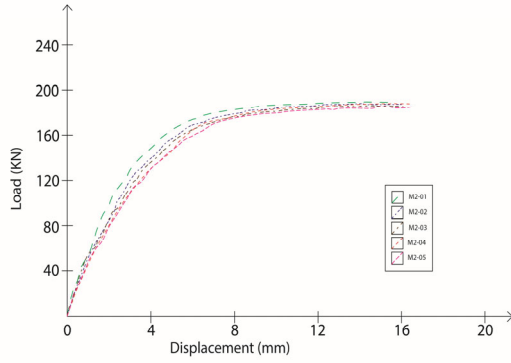


Fig. 5. Load versus displacement graph of the model-2 samples

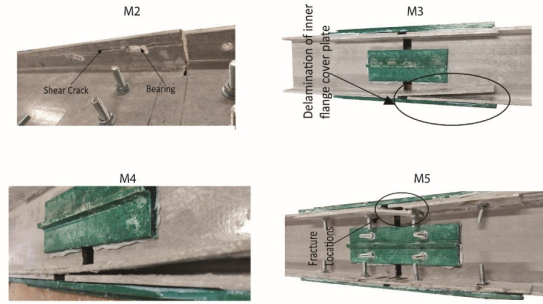


Fig. 6 Failure modes observed in the models

Model-3 and Model-4 are bonded connections, and all samples in both models failed due to cover plate delamination. The model-3 samples had an average maximum load of 44.6 kN and an average displacement of 4.86 mm at failure as given in table 2. The load versus displacement graphs of the model-3 and model-4 samples were shown in Figs. 7 and 8. The average stiffness of the joint is 9.3 kN/mm, with an average compressive strength of 24.38 N/mm². The model-4 samples had an average maximum load of 103.6 kN and an average displacement of 10.1 mm at failure. The joint's average stiffness is calculated to be 13.3 kN/mm, with an average compressive strength of 55.56 N/mm².

Table 2. Specimen’s characteristic properties of model 3 and model 4 samples

Sample ID	Ultimate load (kN)	Displacement at failure (mm)	Stiffness (kN/mm)	Compressive strength (N/mm ²)	Mode of Failure
Model-3					
M3-01	45.5	4.81	9.8	24.85	Delamination
M3-02	45.1	4.83	9.6	24.63	Delamination
M3-03	44.7	4.87	9.4	24.41	Delamination
M3-04	44.1	4.89	9.1	24.09	Delamination
M3-05	43.8	4.92	8.7	23.92	Delamination
Average	44.6	4.86	9.3	24.38	
Model-4					
M4-01	104.4	9.4	13.8	55.98	Delamination
M4-02	104.1	9.9	13.6	55.82	Delamination
M4-03	103.7	10.1	13.4	55.60	Delamination
M4-04	103.2	10.3	13.1	55.34	Delamination
M4-05	102.7	10.9	12.7	55.07	Delamination
Average	103.6	10.1	13.3	55.56	

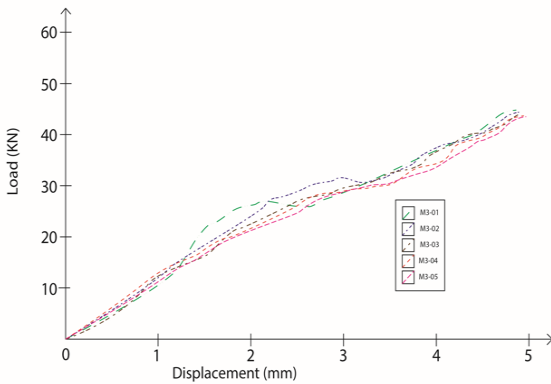


Fig. 7. Load versus displacement graph of the model-3 samples

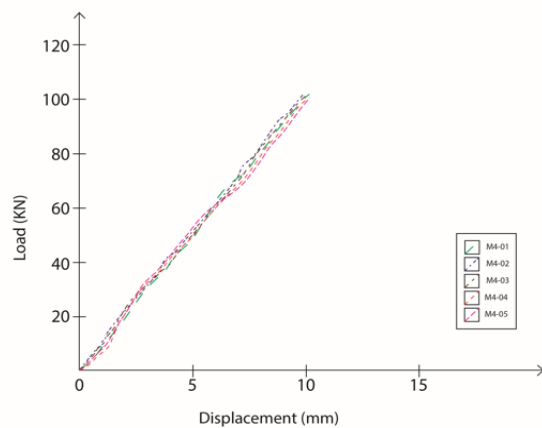


Fig. 8. Load versus displacement graph of the model-4 samples

The strongest connection between the two bonded connections is used to derive model-5. Because the 5 mm thick bond from model-4 samples demonstrated superior joint characteristics compared to the 2 mm thick bond from model-3 samples,

the hybrid connection is designed with a 5 mm thick bond. Load transfer occurs in the web and flange region of model-5 samples, with 20 bolts and 5 mm thick epoxy transmitting load from the upper section of the joint to the lower section, and cover plates providing bearing resistance and bond stiffness. The average maximum load at failure is calculated to be 204.7 kN, with a failure displacement of 14.2 mm as given in table 3. The load versus displacement graph of model-5 was shown in Fig. 9. The average stiffness is calculated to be 22.8 kN/mm, with a compressive strength of 109.75 N/mm² on average. The failure of the connection in these samples is caused primarily by net tension in the joint.

Table 3. Specimen's characteristic properties of model-5 samples

Sample ID	Ultimate load (kN)	Displacement at failure (mm)	Stiffness (kN/mm)	Compressive strength (N/mm ²)	Mode of Failure
M5-01	205.5	13.8	23.2	110.19	Net Tension
M5-02	205.1	13.9	23	109.97	Net Tension
M5-03	204.8	14.2	22.8	109.81	Net Tension
M5-04	204.3	14.4	22.6	109.54	Net Tension
M5-05	203.7	14.9	22.2	109.22	Net Tension
Average	204.7	14.2	22.8	109.75	

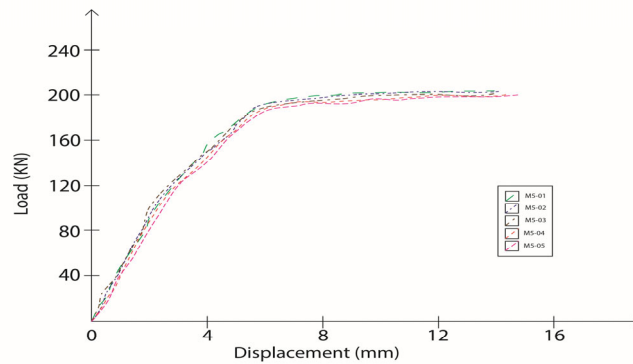


Fig. 9. Load versus displacement graphs of the model-5 samples

Table 4 shows the average maximum load of all models, with the hybrid connection of model-5 exhibiting strength comparable to that of model-1. However, the strongest connection is one made with steel plates, which is due to the modulus of elasticity of the steel plates and steel bolts, which provides superior bearing resistance when compared to GFRP cover plates. The failure in model-1 is primarily due to bearing failure, while the failure in model-5 is primarily due to net tension. The percentage compressive strength to un-cut GFRP H-section short column in model-2 specimens is 82.35%; in model-5 specimens is 89.82%, and in model-1 specimens is 92.83%.

Table 4. Summary of model characteristic properties

Model	Ultimate load (kN)	Compressive strength (N/mm ²)	Percentage Compressive strength to un-cut section (%)
1	211.4	113.43	92.83
2	187.7	100.62	82.35
3	44.6	24.38	19.95
4	103.6	55.56	45.47
5	204.7	109.75	89.82

5. Conclusions

The goal of this study is to improve the design criteria for bonded and hybrid connections in GFRP short splicing columns. Axial loading was applied to 25 GFRP spliced non-bearing connections and 5 un-cut GFRP H-section short columns. The purpose of this experimental study is to determine the primary design principles required to construct a bonded and hybrid non-bearing splicing composite connection of GFRP short H-section columns. The following conclusions were drawn from the present study.

- 1) The load-bearing capacity of the GFRP H-section short column is greater than that of the connections, but because the failure is sudden and abrupt, spliced connections from model-1, model-2, and model-5 are the best alternatives.
- 2) The 5mm thick bond from model-4 samples showed superior joint characteristics compared to the 2mm thick bond from model-3 samples. Bonded connections are more difficult to achieve and take longer to complete than bolted

connections for a variety of reasons, including the avoidance of leakage, the maintenance of bond thickness, the effect of gravity, vertical placement with the casing, and the environment for bond curing.

- 3) Because of the low modulus of elasticity of the GFRP material, the steel bolts sliced through the flange region of the H-section, causing significant bearing and net tension, and resulting in connection failure.
- 4) The joint behavior of the hybrid connection samples, as observed from the load versus displacement graph, demonstrated robustness and significant compressive strength, making them far superior to bonded and bolted connections. This feature of the hybrid connection is caused by the connection providing two load paths with the bond providing a larger surface area for load transfer, thereby significantly reducing the bearing.
- 5) The use of steel bolts for the bolted connection has an effect on the bearing in the joint, which can be reduced by replacing the steel bolts with GFRP bolts, resulting in a homogeneous connection. Because of the bearing resistance provided by steel cover plates, samples from model-1 had a higher compressive strength compared to other models. However, by increasing the thickness of the GFRP plate, the bearing resistance provided by the plates can be increased.

This study is based solely on axial loading conditions, but in practice, eccentric loadings play a significant role in the joint behavior of the connection. Other design advancements, such as using GFRP bolts instead of steel bolts, different patterns of bolted connections, and varying the edge and pitch value, should be researched further.

Acknowledgement

The REVA University provided assistance during the conduct of the tests, which is appreciated by the authors.

References

- Armentani, E., Laiso, M., Caputo, F., & Sepe, R. (2018). Numerical FEM evaluation for the structural behaviour of a hybrid (bonded/bolted) single-lap composite joint. *Procedia Structural Integrity*, 8, 137-153.
- Ascione, F., Feo, L., Lamberti, M., & Penna, R. (2017). Experimental and numerical evaluation of the axial stiffness of the web-to-flange adhesive connections in composite I-beams. *Composite Structures*, 176, 702-714.
- Asdollah-Tabar, M., Heidari-Rarani, M., & Aliha, M. R. M. (2021). The effect of recycled PET bottles on the fracture toughness of polymer concrete. *Composites Communications*, 25, 100684.
- Benedetti, A., Fernandes, P., Granja, J. L., Sena-Cruz, J., & Azenha, M. (2016). Influence of temperature on the curing of an epoxy adhesive and its influence on bond behaviour of NSM-CFRP systems. *Composites Part B: Engineering*, 89, 219-229.
- Chandregowda, S., & Reddy, G. R. C. (2018, April). Evaluation of fastener stiffness modelling methods for aircraft structural joints. In *AIP Conference Proceedings* (Vol. 1943, No. 1, p. 020001). AIP Publishing LLC.
- Choupani, N., & Torun, A. (2022). Fracture characterization of bonded composites: A comparative study. *Engineering Solid Mechanics*, 10(1), 109-116.
- Chowdhury, N. M., Chiu, W. K., Wang, J., & Chang, P. (2016). Experimental and finite element studies of bolted, bonded and hybrid step lap joints of thick carbon fibre/epoxy panels used in aircraft structures. *Composites Part B: Engineering*, 100, 68-77.
- da Silva, L. F., Costa, M., Viana, G., & Campilho, R. D. (2017). Analytical Modelling for the Single-Lap Joint. In *Strength prediction of adhesively-bonded joints* (pp. 8-46). CRC Press.
- Daneshfar, M., Hassani, A., Aliha, M. R. M., & Berto, F. (2017). Evaluating mechanical properties of macro-synthetic fiber-reinforced concrete with various types and contents. *Strength of Materials*, 49, 618-626.
- Daneshfar, M., Hassani, A., Aliha, M. R. M., & Sadowski, T. (2023). Assessment of the Specimen Size Effect on the Fracture Energy of Macro-Synthetic-Fiber-Reinforced Concrete. *Materials*, 16(2), 673.
- de Sousa Marques, E. A., Akhavan-Safar, A., Campilho, R. D. S. G., Carbas, R. J. C., & da Silva, L. F. M. (2019). Advanced numerical models for predicting the load and environmentally dependent behaviour of adhesives and adhesively bonded joints. *State of the Art and Future Trends in Material Modeling*, 211-244.
- Deng, W., Xiong, Y., Liu, D., & Zhang, J. (2019). Static and fatigue behavior of shear connectors for a steel-concrete composite girder. *Journal of Constructional Steel Research*, 159, 134-146.
- Duarte, A. P. C., Sáez, A. D., & Silvestre, N. (2017). Comparative study between XFEM and Hashin damage criterion applied to failure of composites. *Thin-Walled Structures*, 115, 277-288.
- Ezzine, M. C., Amiri, A., Tarfaoui, M., & Madani, K. (2018). Damage of bonded, riveted and hybrid (bonded/riveted) joints, Experimental and numerical study using CZM and XFEM methods. *Advances in aircraft and spacecraft science*, 5(5), 595.
- Figueiredo, J. C. P., Campilho, R. D., Marques, E. A. S., Machado, J. J. M., & da Silva, L. F. M. (2018). Adhesive thickness influence on the shear fracture toughness measurements of adhesive joints. *International Journal of Adhesion and Adhesives*, 83, 15-23.

- Fischer, F., Kreling, S., Jäschke, P., Frauenhofer, M., Kracht, D., & Dilger, K. (2012). Laser surface pre-treatment of CFRP for adhesive bonding in consideration of the absorption behaviour. *The Journal of Adhesion*, 88(4-6), 350-363.
- Galvez, P., Abenobar, J., & Martinez, M. A. (2019). Effect of moisture and temperature on the thermal and mechanical properties of a ductile epoxy adhesive for use in steel structures reinforced with CFRP. *Composites Part B: Engineering*, 176, 107194.
- Gamdani, F., Boukhili, R., & Vadean, A. (2019). Tensile behavior of hybrid multi-bolted/bonded joints in composite laminates. *International Journal of Adhesion and Adhesives*, 95, 102426.
- Gand, A., Mohammed, M., & Jarrouj, S. (2020). Performance of perforated FRP stub beams subject to static transverse actions. *Engineering Solid Mechanics*, 8(2), 105-118.
- Golewski, P., & Sadowski, T. (2017). Investigation of the effect of chamfer size on the behaviour of hybrid joints made by adhesive bonding and riveting. *International Journal of Adhesion and Adhesives*, 77, 174-182.
- Hajiloo, H. R., Karimi, H. R., Aliha, M. R. M., Zanjirani Farahani, H., Salehi, S. M., Hajiloo, M., & Jafari Haghightpour, P. (2022). Crack resistance of fiber-reinforced asphalt mixtures: Effect of test specimen and test condition. *Fatigue & Fracture of Engineering Materials & Structures*, 45(3), 921-937.
- Hississou, R., Seghiri, R., Benzekri, Z., Hilali, M., Rafik, M., & Elharfi, A. (2021). Polymer composite materials: A comprehensive review. *Composite structures*, 262, 113640.
- Iqbal, H. M. S., Bhowmik, S., & Benedictus, R. (2017). Study on the effect of surface morphology on adhesion properties of polybenzimidazole adhesive bonded composite joints. *International Journal of Adhesion and Adhesives*, 72, 43-50.
- Jia, L., Yu, L., Zhang, K., Li, M., Jia, Y., Blackman, B. R. K., & Dear, J. P. (2016). Combined modelling and experimental studies of failure in thick laminates under out-of-plane shear. *Composites Part B: Engineering*, 105, 8-22.
- Karimi, H. R., Aliha, M. R. M., Khedri, E., Mousavi, A., Salehi, S. M., Haghightpour, P. J., & Ebneabbasi, P. (2023). Strength and cracking resistance of concrete containing different percentages and sizes of recycled tire rubber granules. *Journal of Building Engineering*, 106033.
- Kreling, S., Fischer, F., Delmdahl, R., Gäbler, F., & Dilger, K. (2013). Analytical characterization of CFRP laser treated by excimer laser radiation. *Physics Procedia*, 41, 282-290.
- Li, S., Sitnikova, E., Liang, Y., & Kaddour, A. S. (2017). The Tsai-Wu failure criterion rationalised in the context of UD composites. *Composites Part A: Applied Science and Manufacturing*, 102, 207-217.
- Li, W., Guo, S., Giannopoulos, I. K., He, S., & Liu, Y. (2020). Strength enhancement of bonded composite laminate joints reinforced by composite Pins. *Composite Structures*, 236, 111916.
- Liu, F., Lu, X., Zhao, L., Zhang, J., Hu, N., & Xu, J. (2018). An interpretation of the load distributions in highly torqued single-lap composite bolted joints with bolt-hole clearances. *Composites Part B: Engineering*, 138, 194-205.
- Lopez-Cruz, P., Laliberté, J., & Lessard, L. (2017). Investigation of bolted/bonded composite joint behaviour using design of experiments. *Composite Structures*, 170, 192-201.
- Ma, C., Tian, Y., Gong, Y., Zhang, J., Qi, H., & Wang, C. (2018). Study of the effect of curing residual stress on the bonding strength of the single lap joint using a high-temperature phosphate adhesive. *Materials*, 11(7), 1198.
- Marannano, G., & Zuccarello, B. (2015). Numerical experimental analysis of hybrid double lap aluminum-CFRP joints. *Composites Part B: Engineering*, 71, 28-39.
- Mekonen, B., & Bogale, T. (2023). Experimental investigation of tensile, flexural and hardness properties of polyester resin echinatus fiber reinforced composite material. *Engineering Solid Mechanics*, 11(2), 151-162.
- Minghini, F., Tullini, N., Ascione, F., & Feo, L. (2019). Numerical failure analysis of built-up columns composed of closely spaced pultruded FRP channels. *Composite Structures*, 207, 478-487.
- Mohan, J., Ramamoorthy, A., Ivanković, A., Dowling, D., & Murphy, N. (2014). Effect of an atmospheric pressure plasma treatment on the mode I fracture toughness of a co-cured composite joint. *The Journal of Adhesion*, 90(9), 733-754.
- Mousavi, A., Aliha, M. R. M., & Imani, D. M. (2020). Effects of biocompatible Nanofillers on mixed-mode I and II fracture toughness of PMMA base dentures. *Journal of the mechanical behavior of biomedical materials*, 103, 103566.
- Nagavally, R. R. (2017). Composite materials-history, types, fabrication techniques, advantages, and applications. *International Journal of Mechanical and Production Engineering*, 5(9), 82-87.
- Omar, R., Rani, M. A., Yunus, M. A., Mirza, W. W. I., & Zin, M. M. (2018, April). Efficient finite element modelling for the investigation of the dynamic behaviour of a structure with bolted joints. In *AIP Conference Proceedings* (Vol. 1952, No. 1, p. 020082). AIP Publishing LLC.
- Palmieri, F. L., Belcher, M. A., Wohl, C. J., Blohowiak, K. Y., & Connell, J. W. (2016). Laser ablation surface preparation for adhesive bonding of carbon fiber reinforced epoxy composites. *International Journal of Adhesion and Adhesives*, 68, 95-101.
- Paroissien, E., Lachaud, F., Schwartz, S., Da Veiga, A., & Barrière, P. (2017). Simplified stress analysis of hybrid (bolted/bonded) joints. *International Journal of Adhesion and Adhesives*, 77, 183-197.
- Phadnis, V. A., Roy, A., & Silberschmidt, V. V. (2013). A finite element model of ultrasonically assisted drilling in carbon/epoxy composites. *Procedia Cirp*, 8, 141-146.
- Qin, G., Na, J., Tan, W., Mu, W., & Ji, J. (2019). Failure prediction of adhesively bonded CFRP-Aluminum alloy joints using cohesive zone model with consideration of temperature effect. *The Journal of Adhesion*, 95(8), 723-746.
- Quadrino, A., Penna, R., Feo, L., & Nisticò, N. (2018). Mechanical characterization of pultruded elements: Fiber orientation influence vs web-flange junction local problem. Experimental and numerical tests. *Composites Part B: Engineering*, 142, 68-84.

- Ren, Y., Zhang, H., & Xiang, J. (2018). A novel aircraft energy absorption strut system with corrugated composite plate to improve crashworthiness. *International Journal of Crashworthiness*, 23(1), 1-10.
- Ribeiro, F. M. F., Campilho, R. D. S. G., Carbas, R. J. C., & Da Silva, L. F. M. (2016). Strength and damage growth in composite bonded joints with defects. *Composites Part B: Engineering*, 100, 91-100.
- Rooholamini, H., Hassani, A., & Aliha, M. R. M. (2018). Fracture properties of hybrid fibre-reinforced roller-compacted concrete in mode I with consideration of possible kinked crack. *Construction and Building Materials*, 187, 248-256.
- Sadowski, T., & Golewski, P. (2014). Effect of tolerance in the fitting of rivets in the holes of double lap joints subjected to uniaxial tension. In *Key Engineering Materials* (Vol. 607, pp. 49-54). Trans Tech Publications Ltd.
- Sadowski, T., Balawender, T., Golewski, P., Sadowski, T., Balawender, T., & Golewski, P. A. (2015). *Technological aspects of manufacturing and numerical modelling of clinch-adhesive joints* (pp. 1-59). Springer International Publishing.
- Sadowski, T., Kneć, M., & Golewski, P. (2014). Fatigue response of the hybrid joints obtained by hot spot welding and bonding techniques. In *Key Engineering Materials* (Vol. 601, pp. 25-28). Trans Tech Publications Ltd.
- Saeedifar, M., & Zarouchas, D. (2020). Damage characterization of laminated composites using acoustic emission: A review. *Composites Part B: Engineering*, 195, 108039.
- Santos, M. A. S., & Campilho, R. D. S. G. (2018). Experimental and numerical analysis of the fracture envelope of composite adhesive joints. *Science and Technology of Materials*, 30(3), 131-137.
- Tang, H., & Liu, L. (2018). A novel metal-composite joint and its structural performance. *Composite structures*, 206, 33-41.
- Tang, Y., Zhou, Z., Pan, S., Tan, Z., & Wu, H. (2017). Mechanical and failure behavior of three-dimensional six-directional braided composites bolted joint. *Journal of Reinforced Plastics and Composites*, 36(10), 739-753.
- Tao, W., Zhu, P., Xu, C., & Liu, Z. (2020). Uncertainty quantification of mechanical properties for three-dimensional orthogonal woven composites. Part I: Stochastic reinforcement geometry reconstruction. *Composite Structures*, 235, 111763.
- Tao, W., Zhu, P., Xu, C., & Liu, Z. (2020). Uncertainty quantification of mechanical properties for three-dimensional orthogonal woven composites. Part II: Multiscale simulation. *Composite Structures*, 235, 111764.
- Tsokanas, P., Loutas, T., Kotsinis, G., Kostopoulos, V., van den Brink, W. M., & de la Escalera, F. M. (2020). On the fracture toughness of metal-composite adhesive joints with bending-extension coupling and residual thermal stresses effect. *Composites Part B: Engineering*, 185, 107694.
- Wang, G. D., & Melly, S. K. (2018). Three-dimensional finite element modeling of drilling CFRP composites using Abaqus/CAE: a review. *The International Journal of Advanced Manufacturing Technology*, 94, 599-614.
- Xu, C., Liu, Z., Tao, W., & Zhu, P. (2020). A vine copula-based hierarchical framework for multiscale uncertainty analysis. *Journal of Mechanical Design*, 142(3).
- Xu, P., Zhou, Z., Liu, T., Pan, S., Tan, X., Zu, S., & Zhang, Y. (2019). Propagation of damage in bolt jointed and hybrid jointed GLARE structures subjected to the quasi-static loading. *Composite Structures*, 218, 79-94.
- Zhang, D., Zheng, X., & Wu, T. (2019). Damage characteristics of open-hole laminated composites subjected to longitudinal loads. *Composite Structures*, 230, 111474.
- Zhang, J. T., Zhang, M., Li, S. X., Pavier, M. J., & Smith, D. J. (2016). Residual stresses created during curing of a polymer matrix composite using a viscoelastic model. *Composites Science and Technology*, 130, 20-27.
- Zhu, C., Zhu, P., & Liu, Z. (2019). Uncertainty analysis of mechanical properties of plain woven carbon fiber reinforced composite via stochastic constitutive modeling. *Composite Structures*, 207, 684-700.

